Unmanned Systems, Vol. 5, No. 2 (2017) 97–113

DOI: 10.1142/S2301385017500078

UNMANNED SYSTEMS
http://www.worldscientific.com/worldscinet/us

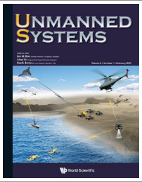

Aggressive Formation Flying of Fixed-Wing UAVs with Differential Geometric Guidance

Arti Kalra[*,§], Sreenatha Anavatti[†,¶], Radhakant Padhi[‡,‖]

[*]Department of Aerospace Engineering,
PEC University of Technology, Chandigarh, India

[†]School of Engineering and Information Technology,
University of New South Wales, Australia

[‡]Department of Aerospace Engineering,
Indian Institute of Science, Bangalore, India

A nonlinear differential geometric guidance scheme is presented in this paper for aggressive autonomous formation flying of fixed-wing unmanned aerial vehicles (UAVs) in the leader-follower framework. It is assumed that the desired location of the followers are known in the velocity frame of the leader. It is also assumed that the followers can also access the position, velocity and acceleration parameters of the leader as necessary auxiliary information. By utilizing this information and manipulating their own dynamics, the proposed logic autonomously guides the followers to their respective desired positions. Depending on the leader's velocity and acceleration information as well as the intended relative location, the formulation also ensures an appropriate direction of the velocity vectors of the followers at the desired relative locations, including its rate of change if any. This leads to minimal transient effects while maintaining the formation even under maneuvering conditions. Usage of quaternions and other innovations ensure that the formulation is singularity-free and hence formation flying is ensured even under aggressive maneuvers of the leader without any restriction on its velocity vector direction. The desired thrust, angle of attack and bank angle are generated using a nonlinear point mass model of a vehicle. The generated guidance commands are then realized using a nonlinear six-DOF model, making the formulation practically more relevant. Extensive simulation studies demonstrate that the proposed approach is capable of bringing the UAVs from arbitrary initial locations to the desired formation and then maintaining the formation even under highly agile motion of the leader.

Keywords: Formation flying; differential geometric guidance; dynamic inversion; unmanned aerial vehicle; UAV.

US

Nomenclature

S_w = Wing planform area (m^2)
b = Wing span (m)
c = Chord length (m)
m = Mass of the UAV (kg)
V_T = Total Velocity of the UAV (m/s)
γ = Flight path angle (deg)
ψ = Heading angle (deg)
α = Angle of attack (deg)
μ = Bank angle (deg)
T = Thrust force (N)
$T_{\max}$ = Maximum thrust force (N)
L = Lift force (N)
D = Drag force (N)
$\bar{q}$ = Dynamic pressure (Pa)
C_L = Lift coefficient
C_D = Drag coefficient
g = Acceleration due to gravity (m/s^2)
ρ = Atmospheric density (Kg/m^3)
C_X, C_Z = Axial coefficient in body axis frame
$k_\gamma, k_\chi, k_{V_T}$ = Gain values of the guidance loop (s^{-1})
k_μ, k_α, k_T = Gain values of the autopilot loop (s^{-1})
T_B^I = Transformation matrix from body to inertial frame
T_V^I = Transformation matrix from velocity to inertial frame

Received 27 August 2016; Revised 15 March 2017; Accepted 15 March 2017; Published 31 July 2017. This paper was recommended for publication in its revised form by editorial board member, Guowei Cai.
Email Addresses: [§]*artikalra257@gmail.com*, [¶]*a.sreenatha@adfa.edu.au*, [‖]*padhi@aero.iisc.ernet.in*

β = Side slip angle (deg)
$T_{V/B}$ = Transformation matrix from body axes to velocity axes

1. Introduction

Formation flying of multiple unmanned aerial vehicles (UAVs) has become a significant topic of research due to numerous defense and commercial applications such as flying into high-risk areas, reconnaissance of wider area, coordinated attacks, livestock monitoring, wildfire mapping, mitigation, etc. to name a few. The key advantage of deploying UAVs is clear from the name itself that there is no necessity of any human resource on board leading to several advantages such as lowering the risk factor significantly, reducing the weight and size of the vehicle leading to efficient flying, shorter runway requirement, etc. In summary, with the deployment of UAVs flight missions can be stretched beyond the conventional domain of operation efficiently.

Formation flying phenomena have been long observed in the natural world. Studies of birds have shown that the V-formation can greatly enhance the overall aerodynamic efficiency by reducing the drag and thereby increasing the endurance [1]. Getting inspired from it, formation flying of aircrafts have been studied as a means to reduce fuel usage by minimizing drag [2]. However, several other mission requirements and advantages as outlined above have generated a lot of interest in this topic. Various approaches such as the standard proportional integral derivative (PID) feedback [3], linear decentralized formation controller [4], peak-seeking controller for optimal relative location [5], and various other guidance logics have been proposed in the literature for formation flying.

It is interesting to observe, to the best of the knowledge of the authors, that most of the logics and philosophies proposed in the literature are based on linear models and/or basic "kinematic" relationships, which ignore the vehicle-specific dynamics of the flying vehicles. Hence, most of these ideas end up with too simplistic results invariably leading to large errors and significant undesirable transient behavior, which is highly undesirable in close formation flying and critical missions. Moreover, some studies impose restrictions on the achievable trajectories and maneuvers by the formation [6, 7], which restricts the domain of formation. Moreover, many formulations consider a few selective motions selected *a priori* and do not allow arbitrary care-free dynamic trajectory change of the leader. Obviously, under such situations online maintenance/reconfiguration of formation for arbitrary motion of the leader turns out to be a demanding (rather impossible) task due to inherent nature of the problem formulation. However, it is obvious that in a realistic dynamic environment, the leader should change its trajectory dynamically to meet the larger mission objective and a good problem formulation must ensure that the followers continue to fly in the given formation along with the leader as naturally as possible (i.e. without exciting erroneous motion during the transient).

An attempt has been made in this paper to address these limitations and propose a fairly generic nonlinear guidance logic using the advanced differential geometric control theory (which is also known as "dynamic inversion") [8]. This facilitates the manipulation of nonlinear point-mass dynamics of the vehicles, which use the vehicle-specific aerodynamic and inertia parameters. Hence the formulation is closer to the reality.

Like most of the problem formulations, the proposed problem formulation here assumes a leader-follower framework. It is assumed that the desired location of the followers are known in the velocity frame of the leader. It is also assumed that the followers can also access the position, velocity and acceleration parameters of the leader as necessary auxiliary information (this information can possibly be broadcast by the leader itself). By utilizing this information and manipulating their own dynamics, the proposed logic then autonomously guides the followers to their respective desired positions. The formulation also computes and ensures appropriate directions of the velocity vectors of the followers at the desired relative location so that the formation is maintained easily without much of transient errors. Usage of quaternions and problem formulation in a unique Cartesian coordinate system (thereby avoiding information conversion between Cartesian and Polar coordinates) ensure that the formulation is singularity-free and hence formation flying is ensured even under aggressive maneuvers of the leader. The desired thrust, angle of attack and bank angle are generated using a nonlinear point mass model of a vehicle, making it practically more relevant. Note that dynamic inversion offers closed form solution in general (or very close to it when nonlinear equations are involved), the solution proposed is computationally quite efficient as well and hence can be implemented in on-board processors.

The use of a six-DOF dynamics for the realization of the guidance commands makes the algorithm more practical. The already generated guidance commands are realized by generating desired body rates, which are finally used to generate control surface deflections making the system more real. Extensive six-DOF simulation studies demonstrate that the proposed approach is capable of bringing the UAVs from arbitrary initial locations to the desired formation and then maintaining the formation irrespective of the highly agile motion of the leader and that too without exciting too much of transient behavior.

Rest of the paper is organized as follows. Section 2 deals with the mathematical model of the physical and aerodynamic properties. Section 3 deals with the formation command generation for followers that includes the use of nonsingular rotation parameter, quaternion. In Sec. 4, simulation results are presented which show that the followers maintain the formation for various motions and maneuvers performed by the leader.

2. Mathematical Model

A pragmatic point-mass model for the All Electric-2 (*AE*-2) UAV [9] has been used in this paper (see Fig. 1). The *AE*-2 UAV is a fixed wing airplane designed for autonomous flying for long endurance. It was designed and developed at the UAV laboratory of the Indian Institute of Science, Bangalore. The thrust is generated by a propeller attached to an electric motor, which is powered by a lithium-polymer battery. The GPS provides the required position information for our algorithm. The implementation has become easier from computational point of view as the vehicle's instrumentation and sensors provide all the necessary information. The geometric and inertial properties with physical attributes of *AE*-2 are given in Table 1.

A full nonlinear six-DOF model for the vehicle is available and has been used earlier for research [10–13]. Since the formulation presented here is concerned with the outermost guidance loop of flight control system, a compatible point-mass model is apposite [14, 15], which can be

Fig. 1. AE-2 (All Electric airplane-2).

Table 1. Physical Data of *AE*-2.

b (m)	c (m)	m (kg)	S_w (m^2)	I_{xx} (kg m^2)	I_{yy} (kg m^2)	I_{zz} (kg m^2)	I_{xz} (kg m^2)
2	0.3	6	0.6	0.5062	0.89	0.91	0.0015

described by the following set of differential equations.

$$\dot{x} = v_x, \tag{1}$$

$$\dot{y} = v_y, \tag{2}$$

$$\dot{z} = v_z, \tag{3}$$

where, x, y and z are the position co-ordinates (in the inertial frame). v_x, v_y and v_z are the velocity vector components representing the velocities in x, y, and z direction, respectively. These velocity components can be expressed in terms of V_T, γ and ψ (representing magnitude of velocity vector, flight path angle and heading angle, respectively) as given below:

$$v_x = V_T \cos\gamma \cos\psi, \tag{4}$$

$$v_y = V_T \cos\gamma \sin\psi, \tag{5}$$

$$v_z = -V_T \sin\gamma. \tag{6}$$

Here V_T can be given as $V_T = \sqrt{v_x^2 + v_y^2 + v_z^2}$. The remaining three equations to complete the set of the mathematical model are obtained by finding the derivatives of Eqs. (1), (2) and (3). Substituting the values of $\dot{V}_T$, $\dot{\gamma}$ and $\dot{\psi}$ from Eqs. (7), (8) and (9), we get the set of differential equations to complete the mathematical model. If we directly use Eqs. (7), (8) and (9), then $\dot{\psi}$ becomes infinite when γ becomes 90. The use of Eqs. (10), (11) and (12) avoids this restriction.

$$\dot{V}_T = \frac{1}{m}(T\cos\alpha - D - mg\sin\gamma), \tag{7}$$

$$\dot{\gamma} = \frac{1}{mV_T}((T\sin\alpha + L)\cos\mu - mg\cos\gamma), \tag{8}$$

$$\dot{\psi} = \frac{1}{mV_T\cos\gamma}(T\sin\alpha + L)\sin\mu, \tag{9}$$

$$\dot{v}_x = \frac{1}{m}\left[\frac{T\sin\alpha + L}{\sqrt{v_x^2 + v_y^2}}\left(\frac{v_z v_x \cos\mu}{V_T} - v_y \sin\mu\right) + \frac{v_x(T\cos\alpha - D)}{V_T}\right], \tag{10}$$

$$\dot{v}_y = \frac{1}{m}\left[\frac{T\sin\alpha + L}{\sqrt{v_x^2 + v_y^2}}\left(\frac{v_z v_y \cos\mu}{V_T} + v_x \sin\mu\right) + \frac{v_y(T\cos\alpha - D)}{V_T}\right], \tag{11}$$

$$\dot{v}_z = \frac{1}{m}\left[\frac{v_z(T\cos\alpha - D)}{V_T} - \frac{\sqrt{v_x^2 + v_y^2}}{V_T} \times (T\sin\alpha + L)\cos\mu + mg\right]. \tag{12}$$

Table 2. Force coefficients of UAV.

C_{X_0}	$C_{X_{\alpha 1}}$	$C_{X_{\alpha 2}}$	C_{Z_0}	$C_{Z_{\alpha 1}}$
0.0386	−0.0040376	−0.0010525	0.1653	0.087138

The computation of aerodynamic forces (drag and lift) is given as

$$D = \bar{q}\ S_w C_D, \tag{13}$$

$$L = \bar{q}\ S_w\ C_L, \tag{14}$$

where the dynamic pressure is given as $\bar{q} = (1/2)\rho V_T^2$. Now the drag and lift forces act on the velocity frame whereas the available aerodynamic forces as sensed by the sensors in the wind tunnel act in the body frame, with the x-axis being pointed backwards [10, 12]. Hence the available forces are transformed into velocity axes by using a suitable transformation matrix, which is as given below

$$\begin{bmatrix} -D \\ -S \\ -L \end{bmatrix} = T_{V/B} \begin{bmatrix} F_{ax} \\ F_{ay} \\ F_{az} \end{bmatrix} = -\bar{q} S_w T_{V/B} \begin{bmatrix} C_X \\ C_Y \\ C_Z \end{bmatrix}, \tag{15}$$

where F_{ax}, F_{ay} and F_{az} are the aerodynamic forces obtained in body axis frame of the vehicle, which is obtained from extensive wind-tunnel testing, followed by curve-fitting (see [12] for details). C_X, C_Y, C_Z are the corresponding force coefficients, respectively. The formulation is carried along with side slip angle $\beta \approx 0$ (which is true as fixed-wing UAV maneuvers are usually done with "turn co-ordination" [13]). The transformation matrix $T_{V/B}$ is given by

$$T_{V/B} = \begin{bmatrix} \cos\alpha & 0 & \sin\alpha \\ 0 & 1 & 0 \\ -\sin\alpha & 0 & \cos\alpha \end{bmatrix}. \tag{16}$$

The force coefficients are further expanded as polynomial functions of angle of attack α and combining those with the explicit expression of $T_{V/B}$ from Eq. (16), the drag and lift coefficients can finally be written as

$$\begin{aligned} D &= \bar{q}S(C_{X_0} + C_{X_{\alpha 1}}\alpha + C_{X_{\alpha 2}}\alpha^2)\cos\alpha \\ &\quad + \bar{q}S(C_{Z_0} + C_{Z_{\alpha 1}}\alpha)\sin\alpha, \\ L &= -\bar{q}S(C_{X_0} + C_{X_{\alpha 1}}\alpha + C_{X_{\alpha 2}}\alpha^2)\sin\alpha \\ &\quad + \bar{q}S(C_{Z_0} + C_{Z_{\alpha 1}}\alpha)\cos\alpha. \end{aligned}$$

Numerical values of the coefficients are given in Table 2 with which the necessary description about the point mass dynamic model for guidance formulation is completed.

3. Nonlinear Guidance for Formation Flying

The main objective of formation flying is to maintain the formation during the complete flight along with following the leader's trajectory. So, a formation command geometry is described according to which the followers are made to fly. The relevant geometric and mathematical formulation for assuring formation flying is described in this section.

3.1. *Generation of formation command for followers*

The formation command for the followers are given from the leader in a virtual velocity frame (that is actually a roll free velocity frame) in terms of three parameters i.e. one relative distance and two geometrical angles. The commanded values to the followers are assumed to be with respect to a virtual reference frame attached to the leader, which actually represents the leader attached virtual velocity frame as shown in Fig. 2.

The x-axis of this frame is aligned to the velocity vector of the leader, whereas y and z contain the velocity roll angle μ and are orthogonal to it as shown in Fig. 2. The relative separation distance is R_d which is having the angle of orientation with the plane and on the plane by the means of ξ and θ, respectively. Hence, the desired position coordinates of follower in leader attached virtual reference frame is given by

$$P_{L,V}^{F_d} = \begin{bmatrix} -R_d \sin\xi \\ R_d \cos\xi \cos\theta \\ -R_d \cos\xi \sin\theta \end{bmatrix}. \tag{17}$$

3.2. *Desired position of follower in local inertial frame*

The position coordinates that are now available in leader attached virtual reference frame are to be transformed into a "local inertial frame" attached to the leader whose orientation is maintained parallel to the earth fixed inertial

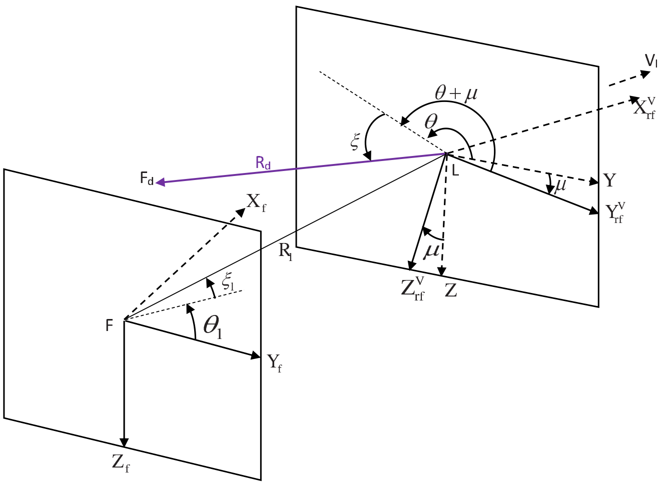

Fig. 2. Formation command geometry in leader's velocity frame.

frame. For calculating the coordinates in this local inertial frame we need to do the transformation through a series of three Euler angle rotations. The desired position coordinates in this local inertial frame are obtained as follows

$$P_{L,I}^{F_d} = [x_{f_d} \quad y_{f_d} \quad z_{f_d}]^T = T_V^I P_{L,V}^{F_d}. \tag{18}$$

The transformation matrix T_V^I is obtained through a series of three Euler angle rotations [15], which is defined as follows

$$T_V^I = T_{\psi_l} T_{\gamma_l} T_{\mu_l}, \tag{19}$$

where,

$$T_{\psi_l} = \begin{bmatrix} \cos\psi_l & -\sin\psi_l & 0 \\ \sin\psi_l & \cos\psi_l & 0 \\ 0 & 0 & 1 \end{bmatrix},$$
$$T_{\gamma_l} = \begin{bmatrix} \cos\gamma_l & 0 & \sin\gamma_l \\ 0 & 1 & 0 \\ -\sin\gamma_l & 0 & \cos\gamma_l \end{bmatrix},$$
$$T_{\mu_l} = \begin{bmatrix} 1 & 0 & 0 \\ 0 & \cos\mu_l & -\sin\mu_l \\ 0 & \sin\mu_l & \cos\mu_l \end{bmatrix}.$$

Representing the 3D rotations with four dimensions makes the transformation linear and easier to manipulate. Hence, all the rotations and their corresponding transformation matrices are represented in quaternions, which is written as a normalized four-dimensional vector. The procedure to calculate the transformation matrix in terms of quaternions, involves the conversion by expressing the quaternion representations in the form of Euler rotations. This is done in the (1–2–3) sequence. The quaternion vector is defined as:

$$q = \begin{bmatrix} q_0 \\ q_1 \\ q_2 \\ q_3 \end{bmatrix}, \tag{20}$$

where,

$$\begin{bmatrix} q_0 \\ q_1 \\ q_2 \\ q_3 \end{bmatrix} = \begin{bmatrix} \cos\frac{\mu_l}{2}\cos\frac{\gamma_l}{2}\cos\frac{\psi_l}{2} - \sin\frac{\mu_l}{2}\sin\frac{\gamma_l}{2}\sin\frac{\psi_l}{2} \\ \sin\frac{\mu_l}{2}\cos\frac{\gamma_l}{2}\cos\frac{\psi_l}{2} + \cos\frac{\mu_l}{2}\sin\frac{\gamma_l}{2}\sin\frac{\psi_l}{2} \\ \cos\frac{\mu_l}{2}\sin\frac{\gamma_l}{2}\cos\frac{\psi_l}{2} - \sin\frac{\mu_l}{2}\cos\frac{\gamma_l}{2}\sin\frac{\psi_l}{2} \\ \cos\frac{\mu_l}{2}\cos\frac{\gamma_l}{2}\sin\frac{\psi_l}{2} + \sin\frac{\mu_l}{2}\sin\frac{\gamma_l}{2}\cos\frac{\psi_l}{2} \end{bmatrix}. \tag{21}$$

Moreover, these quaternion vector components are used after normalization by dividing by L_2 norm of the quaternion components [16]. The transformation matrix can be expressed in quaternions to transform the desired coordinates of the followers to the local inertial frame [17]. The transformation matrix is given by the homogeneous expression as given below, which is multiplied to coordinates of follower in the leader's virtual velocity frame as given in Eq. (18).

$$T_V^I = \begin{bmatrix} q_0^2+q_1^2-q_2^2-q_3^2 & 2(q_1q_2-q_0q_3) & 2(q_0q_2+q_1q_3) \\ 2(q_1q_2+q_0q_3) & q_0^2-q_1^2+q_2^2-q_3^2 & 2(q_2q_3-q_0q_1) \\ 2(q_1q_3-q_0q_2) & 2(q_0q_1+q_2q_3) & q_0^2-q_1^2-q_2^2+q_3^2 \end{bmatrix}. \tag{22}$$

The intention here is to keep tracking the $[x_{f_d}\ y_{f_d}\ z_{f_d}]^T$ while simultaneously keeping in mind the direction of velocity vector of follower as that is not always aligned to that of leader. It can be clearly observed as shown for circular path in Fig. 3. For this objective to be met, the desired position derivatives of follower are obtained by taking the time derivative of the desired position coordinates of the follower in the leader attached local inertial frame as given below

$$\dot{P}_{L,I}^{F_d} = [\dot{x}_{f_d}\ \dot{y}_{f_d}\ \dot{z}_{f_d}]^T = \dot{T}_V^I P_{L,V}^{F_d} + T_V^I \dot{P}_{L,V}^{F_d}. \tag{23}$$

The first term of Eq. (23) is the following vector

$$\dot{T}_V^I P_{L,V}^{F_d} = [\dot{x}_f\ \dot{y}_f\ \dot{z}_f]^T. \tag{24}$$

Without loss of generality, here the commanded variables R_d, ξ and θ are assumed to be constant and hence $P_{L,V}^{F_d}$ is assumed to be a constant vector in magnitude. However, this vector has a rotation effect, which is the reason why $\dot{P}_{L,V}^{F_d}$ is not zero. Instead, the command vector keeps changing dynamically. Hence its rate of change should also

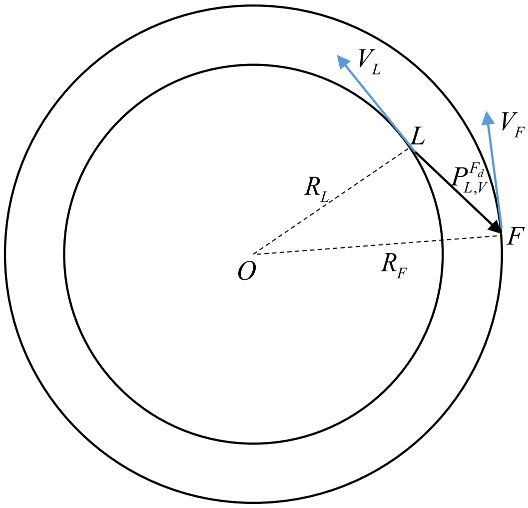

Fig. 3. Velocity alignments in curved motion.

be accounted for, which is calculated as follows

$$\dot{P}^{F_d}_{L,V} = \frac{\partial P^{F_d}_{L,V}}{\partial t} + \omega \times P^{F_d}_{L,V} \tag{25}$$

as the vector is constant,

$$\frac{\partial P^{F_d}_{L,V}}{\partial t} = 0. \tag{26}$$

Hence

$$\dot{P}^{F_d}_{L,V} = \omega \times P^{F_d}_{L,V}, \tag{27}$$

where ω is equal to the angular velocity of leader with respect to the inertial frame. The expression for $\dot{T}^{I}_{V} P^{F_d}_{L,V}$, which is derived from Eqs. (22) and (24), is demonstrated as follows. As it is only a function of quaternion components, q_0, q_1, q_2 and q_3, hence these are written in the form of

$$\dot{x}_f = \frac{\partial x_f}{\partial q_0}\dot{q}_0 + \frac{\partial x_f}{\partial q_1}\dot{q}_1 + \frac{\partial x_f}{\partial q_2}\dot{q}_2 + \frac{\partial x_f}{\partial q_3}\dot{q}_3, \tag{28}$$

$$\dot{y}_f = \frac{\partial y_f}{\partial q_0}\dot{q}_0 + \frac{\partial y_f}{\partial q_1}\dot{q}_1 + \frac{\partial y_f}{\partial q_2}\dot{q}_2 + \frac{\partial y_f}{\partial q_3}\dot{q}_3, \tag{29}$$

$$\dot{z}_f = \frac{\partial z_f}{\partial q_0}\dot{q}_0 + \frac{\partial z_f}{\partial q_1}\dot{q}_1 + \frac{\partial z_f}{\partial q_2}\dot{q}_2 + \frac{\partial z_f}{\partial q_3}\dot{q}_3, \tag{30}$$

where $\dot{x}_f, \dot{y}_f$ and $\dot{z}_f$ are the first order derivatives i.e. the vector as defined in Eq. (24).

The quaternions have to be differentiated for application in the above expression. Since the quaternions are both the function of ψ and γ, they can be differentiated with respect to both and then summed up. This is shown as

$$\dot{q}_n = \frac{\partial q_n}{\partial \gamma}\dot{\gamma} + \frac{\partial q_n}{\partial \psi}\dot{\psi} \quad \text{for } n = 0, 1, 2 \text{ and } 3. \tag{31}$$

The second derivatives of the desired followers position co-ordinates can be obtained in a similar manner to the first derivatives. By differentiating the first order derivatives $\dot{x}_f, \dot{y}_f$ and $\dot{z}_f$, we can obtain $\ddot{x}_f, \ddot{y}_f$ and $\ddot{z}_f$. This can be written as

$$\ddot{x}_f = \frac{\partial \dot{x}_f}{\partial q_0}\ddot{q}_0 + \frac{\partial \dot{x}_f}{\partial q_1}\ddot{q}_1 + \frac{\partial \dot{x}_f}{\partial q_2}\ddot{q}_2 + \frac{\partial \dot{x}_f}{\partial q_3}\ddot{q}_3, \tag{32}$$

$$\ddot{y}_f = \frac{\partial \dot{y}_f}{\partial q_0}\ddot{q}_0 + \frac{\partial \dot{y}_f}{\partial q_1}\ddot{q}_1 + \frac{\partial \dot{y}_f}{\partial q_2}\ddot{q}_2 + \frac{\partial \dot{y}_f}{\partial q_3}\ddot{q}_3, \tag{33}$$

$$\ddot{z}_f = \frac{\partial \dot{z}_f}{\partial q_0}\ddot{q}_0 + \frac{\partial \dot{z}_f}{\partial q_1}\ddot{q}_1 + \frac{\partial \dot{z}_f}{\partial q_2}\ddot{q}_2 + \frac{\partial \dot{z}_f}{\partial q_3}\ddot{q}_3. \tag{34}$$

Note that second derivatives of quaternions have been omitted for brevity.

3.3. *Real position of follower in local inertial frame*

Figure 2 also depicts the follower in its body frame. The line of sight information about the position of leader in its body frame is obtained by the sensors attached to the UAVs. The relative separation between the leader and the follower is the vector R_l which makes an angle ξ_l with the $y_f z_f$ plane, and θ_l is the angle of projection of this vector on $y_f z_f$ with the y_f axis. The position coordinates of leader in follower's body frame are given as below:

$$P^{L}_{F,B} = \begin{bmatrix} R_l \sin \xi_l \\ R_l \cos \xi_l \cos \theta_l \\ -R_l \cos \xi_l \sin \theta_l \end{bmatrix}. \tag{35}$$

The position of leader is then obtained in follower-attached local inertial frame through a series of Euler angles (ψ, θ, ϕ) rotations about z_f, y_f and x_f axes respectively, which is given below:

$$P^{L}_{F,I} = T^{I}_{B} P^{L}_{F,B}, \tag{36}$$

where the transformation matrix T^{I}_{B} is given as

$$T^{I}_{B} = T_{\psi} T_{\theta} T_{\phi}, \tag{37}$$

where,

$$T_{\psi} = \begin{bmatrix} \cos\psi & -\sin\psi & 0 \\ \sin\psi & \cos\psi & 0 \\ 0 & 0 & 1 \end{bmatrix},$$

$$T_{\theta} = \begin{bmatrix} \cos\theta & 0 & \sin\theta \\ 0 & 1 & 0 \\ -\sin\theta & 0 & \cos\theta \end{bmatrix},$$

$$T_{\phi} = \begin{bmatrix} 1 & 0 & 0 \\ 0 & \cos\phi & -\sin\phi \\ 0 & \sin\phi & \cos\phi \end{bmatrix}.$$

The corresponding quaternion vector in terms of Euler angles for the required (body to local inertial) transformation is given below

$$\begin{bmatrix} q_0 \\ q_1 \\ q_2 \\ q_3 \end{bmatrix} = \begin{bmatrix} \cos\frac{\phi}{2}\cos\frac{\theta}{2}\cos\frac{\psi}{2} - \sin\frac{\phi}{2}\sin\frac{\theta}{2}\sin\frac{\psi}{2} \\ \sin\frac{\phi}{2}\cos\frac{\theta}{2}\cos\frac{\psi}{2} + \cos\frac{\phi}{2}\sin\frac{\theta}{2}\sin\frac{\psi}{2} \\ \cos\frac{\phi}{2}\sin\frac{\theta}{2}\cos\frac{\psi}{2} - \sin\frac{\phi}{2}\cos\frac{\theta}{2}\sin\frac{\psi}{2} \\ \cos\frac{\phi}{2}\cos\frac{\theta}{2}\sin\frac{\psi_l}{2} + \sin\frac{\phi}{2}\sin\frac{\theta}{2}\cos\frac{\psi}{2} \end{bmatrix}, \tag{38}$$

whereas the corresponding transformation matrix in terms of quaternion components can be obtained by substituting Eq. (38) in Eq. (22). Now, the actual position of the follower in the leader attached local inertial frame is given as

$$P^{F}_{L,I} = [x\ y\ z]^T = -P^{L}_{F,I}, \tag{39}$$

where $[x\ y\ z]^T$ gives the relative separation of the follower in the leader's local inertial frame. The time derivatives of the position of follower in leader's local inertial frame can be derived as done in Sec. 3.2.

3.4. *Guidance design philosophy for followers*

The fundamental objective of the suggested formulation can be given as:

$$\begin{bmatrix} x \\ y \\ z \end{bmatrix} \rightarrow \begin{bmatrix} x_{f_d} \\ y_{f_d} \\ z_{f_d} \end{bmatrix}, \quad \begin{bmatrix} v_x \\ v_y \\ v_z \end{bmatrix} \rightarrow \begin{bmatrix} v_{x_d} \\ v_{y_d} \\ v_{z_d} \end{bmatrix}. \tag{40}$$

For simplicity, two vectors Z_1 and Z_2 and the error in those variables are first defined as follows

$$Z_1 \equiv \begin{bmatrix} x \\ y \\ z \end{bmatrix}, \quad Z_2 \equiv \begin{bmatrix} v_x \\ v_y \\ v_z \end{bmatrix}, \tag{41}$$

$$\Delta Z_1 \equiv \begin{bmatrix} x - x_{f_d} \\ y - y_{f_d} \\ z - z_{f_d} \end{bmatrix}, \quad \Delta Z_2 \equiv \begin{bmatrix} v_x - v_{x_d} \\ v_y - v_{y_d} \\ v_z - v_{z_d} \end{bmatrix}. \tag{42}$$

The fundamental objective is to make sure that both $\Delta Z_1 \rightarrow 0$ as well as $\Delta Z_2 \rightarrow 0$ simultaneously. With this in mind, first the total tracking error is defined as

$$\Delta Z = \Delta \dot{Z}_1 + K_1 \Delta Z_1, \tag{43}$$

where, K_1 needs to be a positive definite gain matrix (a design tuning parameter) which is given as $K_1 = \mathrm{diag}(k_{1_{11}}, k_{1_{22}}, k_{1_{33}})$. Next, the ideology is taken out to make this tracking error $\Delta Z \rightarrow 0$ asymptotically. It is clearly visible that as $\Delta Z \rightarrow 0$ asymptotically, both $\Delta Z_1 \rightarrow 0$ and $\Delta Z_2 \rightarrow 0$, as in that case only, it would asymptotically lead to stable error dynamics $\Delta \dot{Z}_1 + K_1 \Delta Z_1 = 0$. It leads to the solution $\Delta Z_1(t) = e^{-Kt} \Delta Z_1(t_0) \rightarrow 0$ as $t \rightarrow \infty$, accordingly $\Delta \dot{Z}_1 = -K_1 \Delta Z_1 \rightarrow 0$ as $t \rightarrow \infty$. Moreover, the verification for $\Delta Z_2 \rightarrow 0$ is given as per the given line.

For this, using the definitions of Z_1, Z_2 and defining $f \equiv [v_x\ v_y\ v_z]^T$, it can be observed from the system dynamics Eqs. (1)–(3) that

$$\dot{Z}_1 = f(Z_2) \tag{44}$$

from which one can note that

$$\Delta \dot{Z}_1 = \left[\frac{\partial f(Z_2)}{\partial Z_2}\right] \Delta Z_2, \tag{45}$$

where,

$$\frac{\partial f(Z_2)}{\partial Z_2} \equiv \begin{bmatrix} 1 & 0 & 0 \\ 0 & 1 & 0 \\ 0 & 0 & 1 \end{bmatrix}. \tag{46}$$

It is obvious from Eq. (45) that if $\Delta \dot{Z}_1 = 0$, then $\Delta Z_2 = 0$, provided $\frac{\partial f(Z_2)}{\partial Z_2}$ is nonsingular. However, it is clear from Eq. (46), which is also the biggest advantage of this formulation that this matrix becomes identity, whose inverse never becomes singular.

3.5. *Command generation for followers*

Considering the study undertaken in Sec. 3.4, the basic aim of the guidance loop is to make $\Delta Z \rightarrow 0$ asymptotically. To ensure that, following the philosophy of dynamic inversion [8], the following stable error dynamics is enforced.

$$\Delta \dot{Z} + K_2 \Delta Z = 0, \tag{47}$$

where, K_2 is a positive definite gain matrix (another design tuning parameter), which is given as $K_2 = \mathrm{diag}(k_{2_{11}}, k_{2_{22}}, k_{2_{33}})$. One can extract $\Delta \dot{Z}$ from Eq. (43) as

$$\Delta \dot{Z} = \Delta \ddot{Z}_1 + K_1 \Delta \dot{Z}_1. \tag{48}$$

Substituting Eqs. (43) and (48) in Eq. (47), we get

$$\Delta \ddot{Z}_1 + (K_1 + K_2) \Delta \dot{Z}_1 + K_2 K_1 \Delta Z_1 = 0. \tag{49}$$

Using the definition of ΔZ_1, the above expression is given as follows:

$$\begin{bmatrix} \ddot{x} - \ddot{x}_{f_d} \\ \ddot{y} - \ddot{y}_{f_d} \\ \ddot{z} - \ddot{z}_{f_d} \end{bmatrix} + (K_1 + K_2) \begin{bmatrix} \dot{x} - \dot{x}_{f_d} \\ \dot{y} - \dot{y}_{f_d} \\ \dot{z} - \dot{z}_{f_d} \end{bmatrix} + K_2 K_1 \begin{bmatrix} x - x_{f_d} \\ y - y_{f_d} \\ z - z_{f_d} \end{bmatrix} = 0. \tag{50}$$

However, it can be remarked that

$$[\ddot{x}\ \ddot{y}\ \ddot{z}]^T = \frac{d}{dt}(f(Z_2)) - [\ddot{x}_l\ \ddot{y}_l\ \ddot{z}_l]^T. \tag{51}$$

Executing necessary algebra leads to

$$\begin{bmatrix} \ddot{x} \\ \ddot{y} \\ \ddot{z} \end{bmatrix} = \frac{d}{dt} \begin{bmatrix} v_x \\ v_y \\ v_z \end{bmatrix} - \begin{bmatrix} \ddot{x}_l \\ \ddot{y}_l \\ \ddot{z}_l \end{bmatrix} = A \begin{bmatrix} \dot{v}_x \\ \dot{v}_y \\ \dot{v}_z \end{bmatrix} - \begin{bmatrix} \ddot{x}_l \\ \ddot{y}_l \\ \ddot{z}_l \end{bmatrix}. \tag{52}$$

Substituting Eq. (52) in Eq. (50), the following expression is obtained

$$\begin{bmatrix} \dot{v}_{x_d} \\ \dot{v}_{y_d} \\ \dot{v}_{z_d} \end{bmatrix} = A^{-1} \begin{bmatrix} \ddot{x}_l - \ddot{x}_{f_d} \\ \ddot{y}_l - \ddot{y}_{f_d} \\ \ddot{z}_l - \ddot{z}_{f_d} \end{bmatrix} - A^{-1}(K_1 + K_2)\left(\begin{bmatrix} \dot{x} \\ \dot{y} \\ \dot{z} \end{bmatrix} - \begin{bmatrix} \dot{x}_{f_d} \\ \dot{y}_{f_d} \\ \dot{z}_{f_d} \end{bmatrix} \right) - A^{-1} K_1 K_2 \begin{bmatrix} x - x_{f_d} \\ y - y_{f_d} \\ z - z_{f_d} \end{bmatrix}, \tag{53}$$

where, $A \equiv \frac{\partial f(Z_2)}{\partial Z_2}$. In Eq. (53), $[\dot{x}_{f_d}\ \dot{y}_{f_d}\ \dot{z}_{f_d}]^T$ is computed from Eq. (23), where as $[\dot{x}\ \dot{y}\ \dot{z}]^T$ is computed from system dynamics Eqs. (1)–(3). Note that $\dot{v}_{x_d}$, $\dot{v}_{y_d}$, $\dot{v}_{z_d}$ as obtained in Eq. (53) are the "desired values" of $\dot{v}_x$, $\dot{v}_y$ and $\dot{v}_z$, respectively.

The next task is to generate the desired values of guidance parameters which are thrust T_d, angle of attack α_d and bank angle μ_d. For this objective to met, the following equations hold good

$$\dot{v}_x = \frac{1}{m}\left[\frac{T\sin\alpha + L}{\sqrt{v_x^2+v_y^2}}\left(\frac{v_z v_x \cos\mu}{V_T} - v_y \sin\mu\right) + \frac{v_x(T\cos\alpha - D)}{V_T}\right], \quad (54)$$

$$\dot{v}_y = \frac{1}{m}\left[\frac{T\sin\alpha + L}{\sqrt{v_x^2+v_y^2}}\left(\frac{v_z v_y \cos\mu}{V_T} + v_x \sin\mu\right) + \frac{v_y(T\cos\alpha - D)}{V_T}\right], \quad (55)$$

$$\dot{v}_z = \frac{1}{m}\left[\frac{v_z(T\cos\alpha - D)}{V_T} - \frac{\sqrt{v_x^2+v_y^2}}{v_T} \times (T\sin\alpha + L)\cos\mu + mg\right]. \quad (56)$$

By substituting $\dot{v}_x$, $\dot{v}_y$ and $\dot{v}_z$ by their desired values $\dot{v}_{x_d}$, $\dot{v}_{y_d}$ and $\dot{v}_{z_d}$, respectively in Eqs. (54), (55) and (56), the values for T, α and μ can be solved. These values serve as the desired values of thrust T_d, desired value of angle of attack α_d and desired value of bank angle μ_d, respectively, which are the three guidance parameters.

However, Eqs. (54), (55) and (56) are nonlinear and difficult to solve in closed form. Hence, T_d, α_d and μ_d are generated by using Levenberg–Marquardt and trust-region-reflective methods. While solving for the guidance command parameters, instead of T_d, σ_d is solved where $\sigma = T/T_{\max}$ (where $T_{\max} = 15N$) to avoid numerical ill-conditioning. The initial guess values of the variables are taken as their corresponding "trim values" $T_d = 5.56N$, $\alpha_d = 3.134^\circ$ and $\mu_d = 0^\circ$, respectively (see [12] for details).

It should be observed that bounds were also put on the commanded variables to pacify the vehicle limitations. Numerical values of these bounds are $1.5N \le T_d \le 15N$ for thrust, $-15^\circ \le \alpha_d \le 15^\circ$ for angle of attack and $-60^\circ \le \mu_d \le 60^\circ$ for bank angle.

3.6. *Command generation for the leader*

For simulation studies, it is also required to generate the leader trajectories. It can be observed that there is no desired position command for the leader, thus the argument for the followers to generate their desired velocities do not hold good. Alternatively, it is done in the subsequent manner. It is assumed that the commanded velocity vector components, i.e. v_{x_c}, v_{y_c} and v_{z_c}, respectively, are preferably directly available from the type of maneuver that the leader intends to carry out (in other words, these are the commanded values that the leader receives to guide its own motion). Based on this information, the desired values of velocity $\dot{v}_{x_d}$, $\dot{v}_{y_d}$ and $\dot{v}_{z_d}$ are generated according to the following first-order autopilot loops

$$\dot{v}_x = -k_{v_x}(v_{x_d} - v_{x_c}), \quad (57)$$

$$\dot{v}_y = -k_{v_y}(v_{y_d} - v_{y_c}), \quad (58)$$

$$\dot{v}_z = -k_{v_z}(v_{z_d} - v_{z_c}), \quad (59)$$

where $k_{v_x} > 0$, $k_{v_y} > 0$ and $k_{v_z} > 0$ are the gain values that need to be tuned carefully. Next, the desired values of $\dot{v}_{x_d}$, $\dot{v}_{y_d}$ and $\dot{v}_{z_d}$ are used to compute the desired guidance parameters that are desired thrust T_d, desired angle of attack α_d and desired bank angle μ_d, respectively, which is done exactly as per the procedure described for the followers using Eqs. (54), (55) and (56).

4. Simulation Results

For simulation studies, we have taken one leader aircraft and four followers. Furthermore, all five were considered to be alike UAV models of AE-2 (see Sec. 2 for details about it). The first-order autopilot loops are incorporated in the guidance commands to show the actual scenario. The formation flight control system's response to the leader's maneuvers and command changes as described in Sec. 3 in the formation geometry were simulated and scrutinized.

4.1. *Six-DOF dynamics*

Although point mass model was quite appropriate for guiding the vehicles to the desired trajectories, a more realistic approach was followed. To make the system more practical, the achieved guidance commands were realized by generating rate limits of fin deflections, the algorithm for which is explained further. Although, it was not hard because of the prior knowledge [11]. To make the algorithm more practical and have better simulation results, the generated guidance commands are now used in a six-DOF model to predict the desired body rates, which are then tracked by generating control surface deflections making it more real. The six-DOF equations of motion for the UAV can be written as the following set of equations, where the first three equations are same as Eqs. (1), (2) and (3). The next three equations [Eqs. (63), (64) and (65)] are obtained in a similar manner as in the point mass dynamics, i.e. by differentiating Eqs. (1), (2) and (3) and substituting the values of $\dot{V}_T$, $\dot{\gamma}$ and $\dot{\psi}$ from Eqs. (60), (61) and (62).

$$\dot{V}_T = (T\cos\alpha\cos\beta + F_{ax}\cos\alpha\cos\beta)/m + (F_{ay}\sin\beta + F_{az}\sin\alpha\cos\beta)/m - g\sin\gamma, \tag{60}$$

$$\dot{\gamma} = \frac{-g\cos\gamma}{V_T} + \frac{T+F_{ax}}{mV_T}(\sin\alpha\cos\mu + \cos\alpha\sin\beta\sin\mu) - \frac{F_{ay}\cos\beta\sin\mu}{mV_T} + \frac{F_{az}}{mV_T}(\sin\alpha\sin\beta\sin\mu - \cos\alpha\cos\mu), \tag{61}$$

$$\dot{\psi} = \frac{T+F_{ax}}{mV_T\cos\gamma}(\sin\alpha\sin\mu - \cos\alpha\sin\beta\cos\mu) - \left(\frac{F_{az}}{mV_T}\right) \times \sec\gamma(\cos\alpha\sin\mu + \sin\alpha\sin\beta\cos\mu) + \frac{F_{ay}\cos\beta\cos\mu}{mV_T\cos\gamma}, \tag{62}$$

$$\begin{aligned}\dot{v}_x = {} & \frac{v_x}{mV_T}(T\cos\alpha\cos\beta + F_{ax}\cos\alpha\cos\beta + F_{ay}\sin\beta + F_{az}\sin\alpha\cos\beta) + \frac{v_x v_z}{mV_T\sqrt{v_x^2+v_y^2}} \\ & \times \{(T+F_{ax})(\sin\alpha\cos\mu + \cos\alpha\sin\beta\sin\mu) - F_{ay}\cos\beta\sin\mu + F_{az} \times (\sin\alpha\sin\beta\sin\mu - \cos\alpha\cos\mu)\} \\ & - \frac{v_y}{m\sqrt{v_x^2+v_y^2}}\{(T+F_{ax})(\sin\alpha\sin\mu - \cos\alpha\sin\beta\cos\mu) + F_{ay}\cos\beta\cos\mu - F_{az}(\sin\alpha\sin\beta\cos\mu + \cos\alpha\sin\mu)\},\end{aligned} \tag{63}$$

$$\begin{aligned}\dot{v}_y = {} & \frac{v_y}{mV_T}(T\cos\alpha\cos\beta + F_{ax}\cos\alpha\cos\beta + F_{ay}\sin\beta + F_{az}\sin\alpha\cos\beta) + \frac{v_y v_z}{mV_T\sqrt{v_x^2+v_y^2}}\{(T+F_{ax}) \\ & \times (\sin\alpha\cos\mu + \cos\alpha\sin\beta\sin\mu) - F_{ay}\cos\beta\sin\mu + F_{az}(\sin\alpha\sin\beta\sin\mu - \cos\alpha\cos\mu)\} \\ & + \frac{v_x}{m\sqrt{v_x^2+v_y^2}}\{(T+F_{ax})(\sin\alpha\sin\mu - \cos\alpha\sin\beta\cos\mu) + F_{ay}\cos\beta\cos\mu - F_{az}(\sin\alpha\sin\beta\cos\mu + \cos\alpha\sin\mu)\},\end{aligned} \tag{64}$$

$$\begin{aligned}\dot{v}_z = {} & \frac{v_z}{mV_T}(T\cos\alpha\cos\beta + F_{ax}\cos\alpha\cos\beta + F_{ay}\sin\beta + F_{az}\sin\alpha\cos\beta) - \frac{\sqrt{v_x^2+v_y^2}}{mV_T}\{(T+F_{ax}) \\ & \times (\sin\alpha\cos\mu + \cos\alpha\sin\beta\sin\mu) - F_{ay}\cos\beta\sin\mu + F_{az}(\sin\alpha\sin\beta\sin\mu - \cos\alpha\cos\mu)\} + g,\end{aligned} \tag{65}$$

$$\dot{P} = c_1RQ + c_2PQ + c_3L_a + c_4N_a, \tag{66}$$

$$\dot{Q} = c_5PR - c_6(P^2 - R^2) + c_7(M_a + M_{th}), \tag{67}$$

$$\dot{R} = c_8PQ - c_2RQ + c_4L_a + c_9N_a, \tag{68}$$

$$\dot{\beta} = P\sin\alpha - R\cos\alpha + \left(\frac{\sqrt{v_x^2+v_y^2}}{V_T^2}\right)g\sin\mu - \left(\frac{1}{mV_T}\right) \times ((F_{ax}+T)\cos\alpha\sin\beta - F_{ay}\sin\beta + F_{az}\sin\alpha\sin\beta), \tag{69}$$

where, x, y and z are the position co-ordinates and P, Q and R are the roll, pitch and yaw rates, respectively. v_x, v_y and v_z are the velocity vector components representing the velocities in x, y and z directions, respectively which are given in Eqs. (4), (5) and (6). The aerodynamic forces (F_{ax}, F_{ay}, F_{az}), aerodynamic moments (L_a, M_a, N_a), and moment due to the thrust offset from the aircraft's CG (M_{th}) are given as follows:

$$\begin{bmatrix} F_{ax} \\ F_{ay} \\ F_{az} \end{bmatrix} = -\bar{q}S_w \begin{bmatrix} C_X \\ C_Y \\ C_Z \end{bmatrix}, \tag{70}$$

$$\begin{bmatrix} L_a \\ M_a \\ N_a \end{bmatrix} = \bar{q}S_w \begin{bmatrix} bC_l \\ cC_m \\ bC_n \end{bmatrix}, \tag{71}$$

$$M_{th} = -dT, \tag{72}$$

where b, c and S_w represent the wing span, chord length and wing planform area of the aircraft, respectively, and $\bar{q}$ is the free stream dynamic pressure. T represents thrust produced, where d is the offset of the thrust line from the aircraftâĂŹs CG.

4.1.1. *Autopilot synthesis*

The response of the vehicle airframe is not prompt, when the desired thrust T_d, desired angle of attack α_d and desired bank angle μ_d are issued to a vehicle as the guidance commands. It rather gradually achieves the commanded values as the commanded values are realized through first-order autopilot dynamics.

$$\dot{T} = -k_T(T - T_d), \tag{73}$$

$$\dot{\mu} = -k_\mu(\mu - \mu_d), \tag{74}$$

$$\dot{\alpha} = -k_\alpha(\alpha - \alpha_d), \tag{75}$$

$$\dot{\beta} = -k_\beta(\beta - \beta_d). \tag{76}$$

The gain values for autopilot dynamics $k_T > 0, k_\alpha > 0, k_\mu > 0$ and $k_\beta > 0$ are chosen high enough so that the settling time of this loop is smaller than that of the outer loop guidance. Equation (73) simply represents an approximate engine dynamics for the motion of the UAV.

4.1.2. *Outer loop*

The desired body rates are generated in this loop using Eqs. (74), (75) and (76). Equation (76) is used to ensure that the follower always performs coordinated turns, the angle of sideslip β should be maintained at zero and the value of k_β is taken as $2\,\mathrm{s}^{-1}$. Because β is required to be zero so the desired value β_d is set to be zero. By substituting the values of $\dot{\mu}$, $\dot{\alpha}$ and $\dot{\beta}$ in Eqs. (74), (75) and (76) as given below, the values for desired body rates can be solved.

$$\begin{aligned}\dot{\mu} = {} & \frac{P\cos\alpha}{\cos\beta} + \frac{R\sin\alpha}{\cos\beta} - g\cos\mu\tan\beta\left(\frac{\sqrt{v_x^2+v_y^2}}{V_T^2}\right)\\ & + \left(\frac{T+F_{ax}}{mV_T}\right)\left(\sin\alpha\tan\beta - \left(\frac{v_z}{\sqrt{v_x^2+v_y^2}}\right)\right.\\ & \left.\times(\sin\alpha\sin\mu - \cos\alpha\sin\beta\cos\mu)\vphantom{\frac{v_z}{\sqrt{v_x^2}}}\right)\\ & - \frac{1}{mV_T}\left(F_{ay}\cos\beta\cos\mu\left(\frac{v_z}{\sqrt{v_x^2+v_y^2}}\right)\right) - \left(\frac{F_{az}}{mV_T}\right)\\ & \times\left(\cos\alpha\tan\beta - \left(\frac{v_z}{\sqrt{v_x^2+v_y^2}}\right)\right.\\ & \left.\times(\cos\alpha\sin\mu + \sin\alpha\sin\beta\cos\mu)\vphantom{\frac{v_z}{\sqrt{v_x^2}}}\right),\end{aligned} \tag{77}$$

$$\begin{aligned}\dot{\alpha} = {} & -P\cos\alpha\tan\beta + Q - R\sin\alpha\tan\beta + \left(\frac{\sec\beta}{V_T}\right)\\ & \times\left(g\cos\mu\left(\frac{\sqrt{v_x^2+v_y^2}}{V_T}\right)\right.\\ & \left.-\frac{1}{m}((T+F_{ax})\sin\alpha - F_{az}\cos\alpha)\right),\end{aligned} \tag{78}$$

$$\begin{aligned}\dot{\beta} = {} & P\sin\alpha - R\cos\alpha + \left(\frac{\sqrt{v_x^2+v_y^2}}{V_T^2}\right)g\sin\mu - \left(\frac{1}{mV_T}\right)\\ & \times((F_{ax}+T)\cos\alpha\sin\beta - F_{ay}\sin\beta + F_{az}\sin\alpha\sin\beta).\end{aligned} \tag{79}$$

The above equations are solved for P, Q and R which are interpreted as desired body rates, P_d, Q_d and R_d for the next loop. Hence, the desired body rates $U_C = [P_d\, Q_d\, R_d]^T$ are obtained separating the state and control terms in $\dot{\mu}$, $\dot{\alpha}$ and $\dot{\beta}$ from Eqs. (77), (78) and (79) as follows:

$$f_C + g_C U_C = b_C. \tag{80}$$

One important point to note here is that Eqs. (77), (78) and (79) contain terms containing forces which indirectly contain the control deflections which are yet to be calculated in the inner most loop. So here, the previously assumed values of aerodynamic control deflections are used. The terms f_C, g_C and b_C are defined appropriately, details of which are omitted here for brevity. From Eq. (83), assuming g_C to be nonsingular, it can be clearly seen that

$$U_C = g_C^{-1}(b_C - f_C). \tag{81}$$

4.1.3. *Inner loop*

The inner most loop takes the desired body rates as input and generates the necessary aerodynamic control surface deflections that are required to achieve those desired angular rates, which represents a more realistic form of already generated guidance commands. The objective of this loop is $[P\ Q\ R]^T \to [P_d\ Q_d\ R_d]^T$. Moreover, it uses a faster DI controller as compared to the controller used for computing the desired body rates. The aerodynamic control surface deflections are generated in such a way that the desired body rates are tracked. To achieve the objective, the following first-order dynamics is enforced:

$$\begin{bmatrix}\dot{P}-\dot{P}_d\\ \dot{Q}-\dot{Q}_d\\ \dot{R}-\dot{R}_d\end{bmatrix} + \begin{bmatrix}k_P & 0 & 0\\ 0 & k_Q & 0\\ 0 & 0 & k_R\end{bmatrix}\begin{bmatrix}P-P_d\\ Q-Q_d\\ R-R_d\end{bmatrix} = 0, \tag{82}$$

where $\dot{P}_d$, $\dot{Q}_d$ and $\dot{R}_d$ are assumed to be zero (quasi-steady approximation). The control deflections $U_C = [\delta_a\ \delta_e\ \delta_r]^T$ are obtained separating the state and control terms in $\dot{P}$, $\dot{Q}$ and $\dot{R}$ from Eq. (66), (67) and (68) as follows:

$$f_C + g_C U_C = b_C. \tag{83}$$

The terms f_C, g_C and b_C are defined appropriately, details of which are omitted here for brevity. From Eq. (83), assuming

g_C to be nonsingular, it can be clearly seen that

$$U_C = g_C^{-1}(b_C - f_C). \tag{84}$$

As we know the response in DI controller design can be controlled by the appropriate selection of gain values. The gain values are selected in order to enforce the desired settling time requirements.

4.2. *Selection of design parameters and initial conditions*

The simulation studies are carried out for two different formation geometries where the followers fly behind the leader (1) in a triangular shape, (2) in conical shape as shown in Figs. 4 and 5 whereas the demonstration of the results for the conical formation have been omitted in this paper for brevity. The relative position commands for formation flying (see Sec. 3) taken for the simulation studies is given in Tables 3 and 5 (given $OL = 100$ m in Fig. 5), which was kept constant irrespective of the maneuver of the leader for a particular flight. Even, studies are done for a tight formation as given in Table 3 and for helical (circular) motion, results for a relatively loose formation has been demonstrated (Table 4).

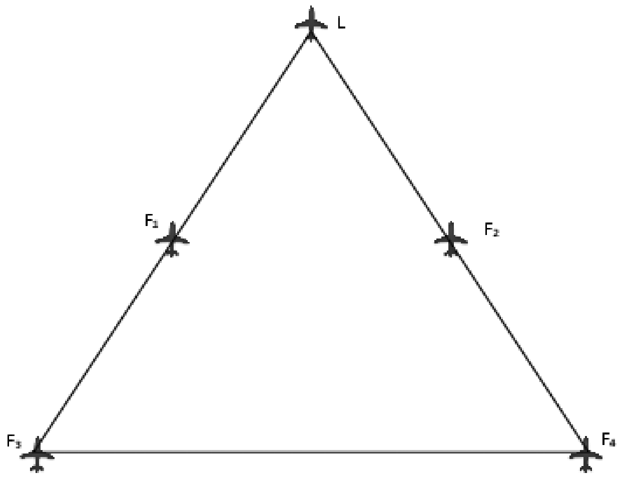

Fig. 4. Triangular formation design with four followers.

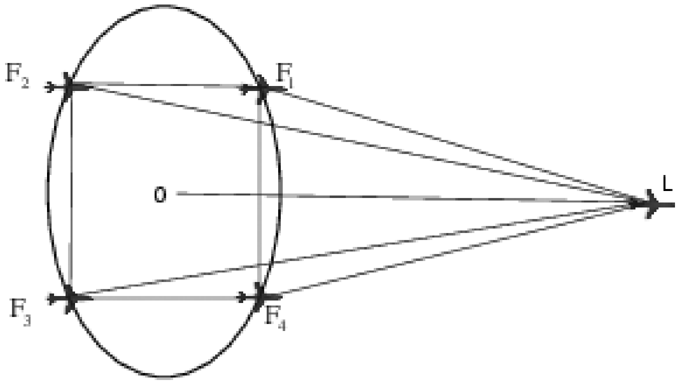

Fig. 5. Conical formation design with four followers.

Table 3. Formation command for triangular formation (tight).

Follower–1	R = 10 m	$\theta = 0°$	$\xi = 135°$
Follower–2	R = 20 m	$\theta = 0°$	$\xi = 45°$
Follower–3	R = 10 m	$\theta = 0°$	$\xi = 135°$
Follower–4	R = 20 m	$\theta = 0°$	$\xi = 45°$

Table 4. Formation command for triangular formation (loose).

Follower–1	R = 50 m	$\theta = 0°$	$\xi = 135°$
Follower–2	R = 100 m	$\theta = 0°$	$\xi = 45°$
Follower–3	R = 50 m	$\theta = 0°$	$\xi = 135°$
Follower–4	R = 100 m	$\theta = 0°$	$\xi = 45°$

The initial position of leader is taken as $Z_L(0) = [400\text{m}\ 600\text{m}\ -100\text{m}]^T$ (note that negative Z means positive height). Similarly, the magnitude of initial velocity vector of the leader was taken as $V_L(0) = 20$ m/s. The initial values of the flight path angle and heading angle are taken as $\gamma(0) = 5°\psi(0) = 0°$. Hence, the initial components of velocity in x, y and z direction can be calculated using Eqs. (4), (5) and (6), respectively. To demonstrate the effectiveness of the proposed approach, the selection of initial conditions is done in such a way that the initial error of the followers is adequately a large value when compared to that of the leader so that the follower can come into the given formation taking ample settling time.

The initial conditions for the followers are given in Table 6. The velocities in x, y and z directions can be computed using the relations in Eqs. (4), (5) and (6).

Numerical values of the gains are chosen appropriately to suit the settling time requirements.The selected controller gain values are given in Table 7.

It can be mentioned here that combination of Eqs. (43) and (47) and selection of diagonal K_1 and K_2 lead to second order dynamics in each error channel with damping ratios being greater than unity. This means that the closed loop

Table 5. Formation command for conical formation.

Follower–1	R = 111.8 m	$\theta = 135°$	$\xi = 63.5°$
Follower–2	R = 111.8 m	$\theta = 45°$	$\xi = 63.5°$
Follower–3	R = 111.8 m	$\theta = 225°$	$\xi = 63.5°$
Follower–4	R = 111.8 m	$\theta = 315°$	$\xi = 63.5°$

Table 6. Initial conditions for triangular formation.

Variable	Velocity V_T	Position (x, y, z)	Euler angles (μ, γ, ψ)
Follower 1	$V_t = 18\,\mathrm{m/s}$	$(300, 700, -100)$	$(0, 0, 30)$
Follower 2	$V_t = 18\,\mathrm{m/s}$	$(300, 500, -100)$	$(0, 0, -30)$
Follower 3	$V_t = 18\,\mathrm{m/s}$	$(200, 800, -100)$	$(0, 0, 30)$
Follower 4	$V_t = 18\,\mathrm{m/s}$	$(200, 400, -100)$	$(0, 0, -30)$

Table 7. Selection of gain values.

Parameter	$k_{1_{11}}$	$k_{1_{22}}$	$k_{1_{33}}$
Gain values	$0.09\,\mathrm{s}^{-1}$	$0.09\,\mathrm{s}^{-1}$	$0.09\,\mathrm{s}^{-1}$
Parameter	$k_{2_{11}}$	$k_{2_{22}}$	$k_{2_{33}}$
Gain values	$0.04\,\mathrm{s}^{-1}$	$0.04\,\mathrm{s}^{-1}$	$0.04\,\mathrm{s}^{-1}$
Parameter	k_T	k_α	k_μ
Gain values	$3\,\mathrm{s}^{-1}$	$15\,\mathrm{s}^{-1}$	$15\,\mathrm{s}^{-1}$
Parameter	k_P	k_Q	k_R
Gain values	$10\,\mathrm{s}^{-1}$	$10\,\mathrm{s}^{-1}$	$10\,\mathrm{s}^{-1}$

system behaves like "over-damped" second-order system and hence the probability of collision among the followers and leader is least due to the absence of any over-shooting.

4.3. *Unique path command for the leader*

In this section, only single type of path command is given to the leader to fly and we are analyzing the performance for a specified simulation time. Several kinds of paths in different formation geometries are discussed in the following sections.

4.3.1. *Case 1: Sinusoidal trajectory*

We have tried to demonstrate the behavior of followers in a formation pattern in which the formation is assumed to undergo a sinusoidal maneuver while taking off (which contains both lateral and longitudinal maneuver). The command given to leader to perform this path is in terms of velocity components assumed to be the following:

$$V_{T_c} = 20\,\mathrm{m/s}, \tag{85}$$

$$\gamma_c = 5^\circ, \tag{86}$$

$$\psi_c = \sin\left(\frac{2\pi t V_{T_c}}{L_s}\right), \tag{87}$$

where L_s gives the total distance covered by the leader in forward direction for one complete cycle of sinusoidal. The 3D plot of the leader and followers performing given

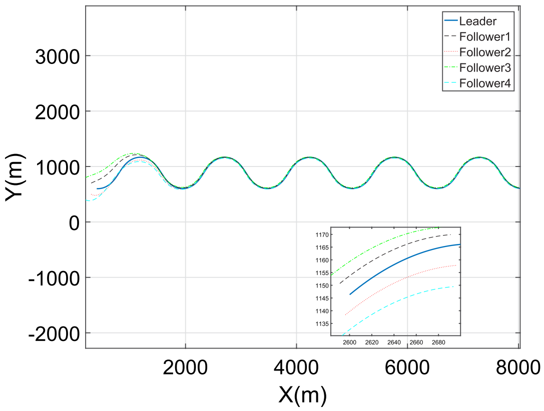

Fig. 6. Two-dimensional planar view for sinusoidal trajectory.

maneuver is shown in Fig. 6. It can be remarked from Fig. 7 that the desired relative distance is attained between the leader and the individual followers. It can be observed from the errors in velocity between leader and the followers (Fig. 8) that the velocity of the followers are not really aligned to that of the leader. It can be seen from Fig. 9 that the controls are within their bounds. The plots for yaw, pitch and roll rates for sinusoidal trajectory are shown in Fig. 10. Figure 11 shows that the control deflections are also within their respective bounds.

4.3.2. *Case 2: Helical climb-up motion*

In this section, a relatively onerous case is presented where the leader executes a combined longitudinal and lateral helical climb-up motion in a relatively loose formation. The aircrafts perform circular loops along with a continuous rise in altitude so that its trajectory forms a helix in 3D. The commands given to leader are generated from these values:

$$V_{T_c} = 20\,\mathrm{m/s}, \tag{88}$$

$$\gamma_c = 5^\circ, \tag{89}$$

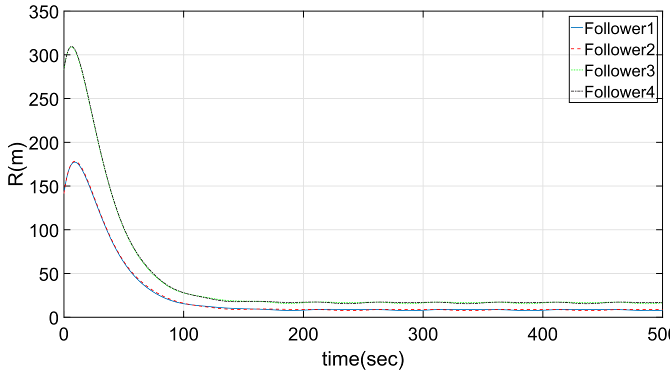

Fig. 7. Relative distance history between individual followers and leader for sinusoidal trajectory.

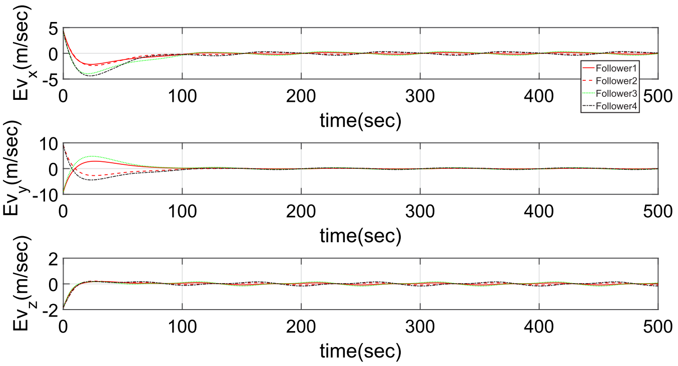

Fig. 8. Error in velocity components between leader and follower for sinusoidal trajectory.

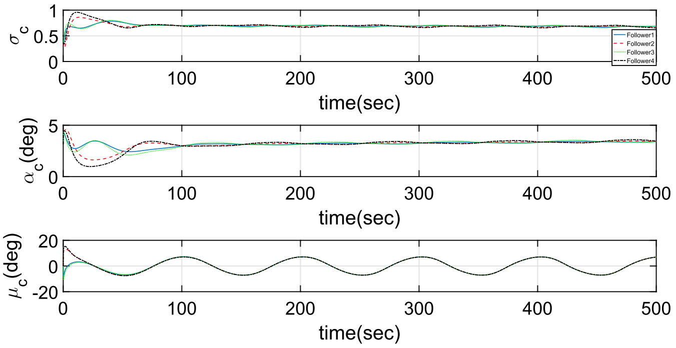

Fig. 9. Thrust, Angle of attack and Bank angle of UAVs for sinusoidal trajectory.

$$\psi_c = tV_{T_c}/R_c \text{ radians}, \tag{90}$$

where R_c is the radius of the circle to be executed by the leader (which is taken here as "1000 m") and "t" is the instantaneous time in seconds. The results obtained are shown in Figs. 12–16.

From Fig. 12, one can see that with the application of the proposed guidance, the followers from the arbitrary locations are able to come and join the leader to perform the helical maneuver along with it in the given formation.

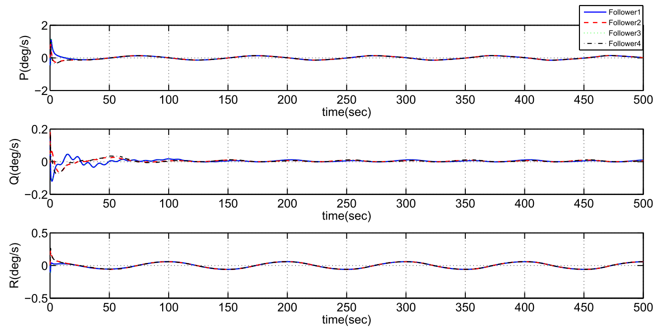

Fig. 10. Angular rates for sinusoidal trajectory.

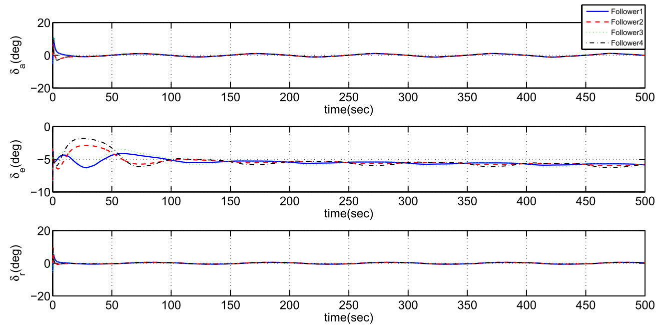

Fig. 11. Elevator, aileron and rudder deflections for sinusoidal trajectory.

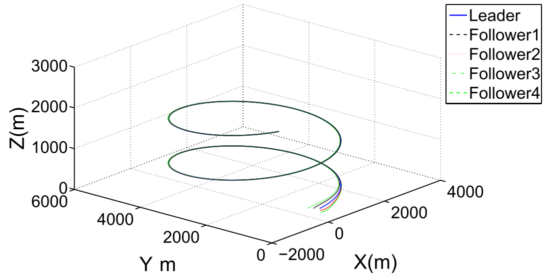

Fig. 12. Three-dimensional view for helical climb-up trajectory.

Figure 13 gives a better picture of this behavior in the horizontal planar view (only one circular motion is shown for better clarity). One can notice that the error value is growing first before declining. This is because of the initial error in the magnitude and orientation of the velocity vectors which is quite different from their corresponding desired values. Figure 15 shows how the errors between the velocity vector components of the leader and the follower are not exactly zero, especially in curved paths as there is a small rotational component that alters the direction of velocity of follower with respect to the leader. As mentioned before, this is a key feature of the proposed algorithm.

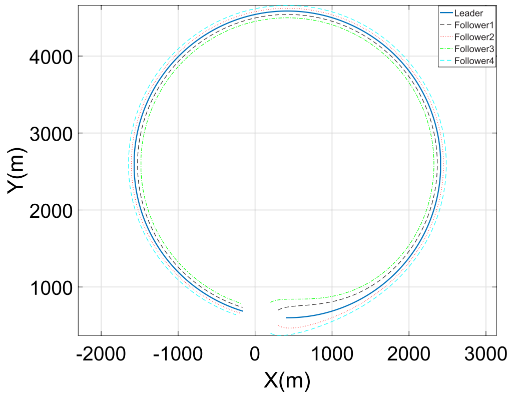

Fig. 13. Two-dimensional planar view for helical motion.

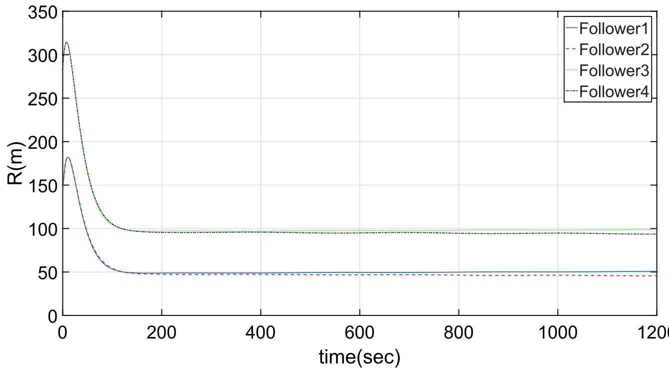

Fig. 14. Relative distance history between individual followers and leader for helical motion.

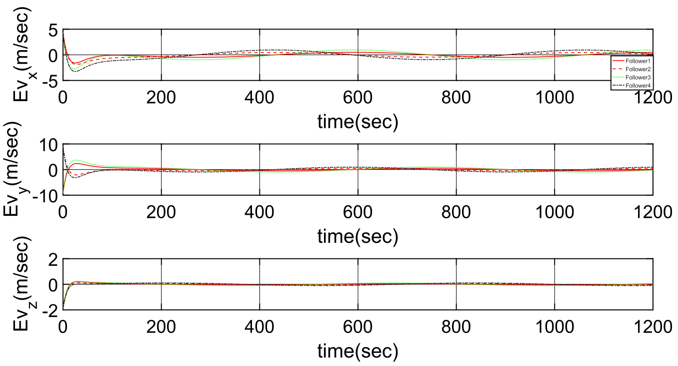

Fig. 15. Error in velocity components between leader and two followers for helical motion.

A comparison has been made with the previous studies when velocity of follower and leader was aligned (as shown in Fig. 14). As in earlier studies the second term in the Eq. (23) was taken zero. The study has been done for followers 1 and 3 considering the rotational effects while neglecting for followers 2 and 4. It can be observed from Fig. 14 that the errors in relative distances have been reduced than earlier for followers 1 and 3 in comparison to followers 2 and 4.

The executed physical parameters, namely the thrust angle of attack and bank angle for all the five vehicles are plotted in Fig. 16 which shows that all these values are within the capability limits of the vehicle. The plots for yaw, pitch and roll rates are shown in Fig. 17. Also, Fig. 18 shows that the aerodynamic control surface deflections lie within the limits of the vehicle.

However, one can note that the thrust value of Follower-2 and Follower-4 is close to the bound of $15N$. This is because of the fact that initially its location is a bit far away and it has to speed up a bit to catch up with the desired location (see Fig. 14 for a better view of this fact).

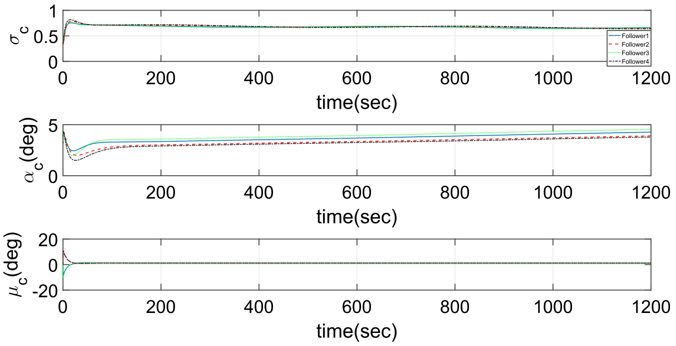

Fig. 16. Thrust, Angle of attack and Bank angle of UAVs for helical motion.

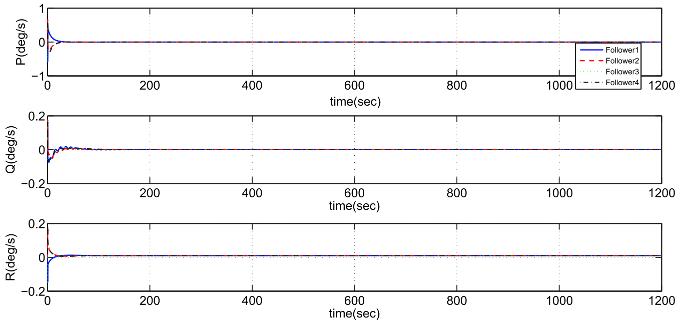

Fig. 17. Angular rates for helical motion.

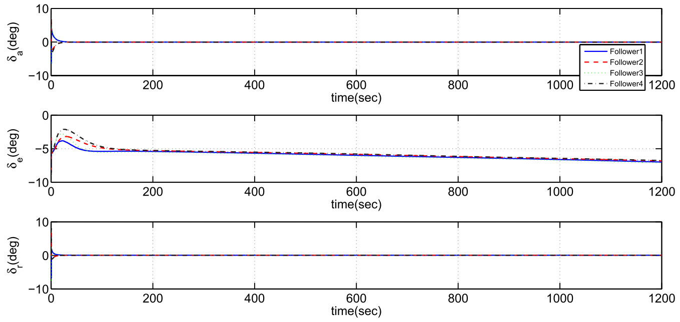

Fig. 18. Elevator, aileron and rudder deflections for helical motion.

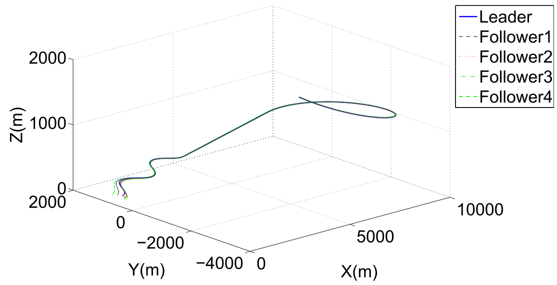

Fig. 19. Three dimensional view for formation flying with sequential multiple commands to the leader.

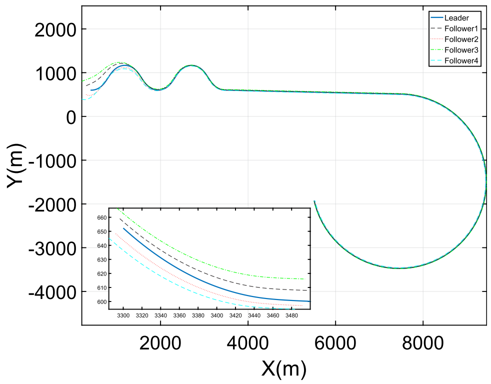

Fig. 20. Two-dimensional planar view for formation flying with sequential multiple commands to the leader.

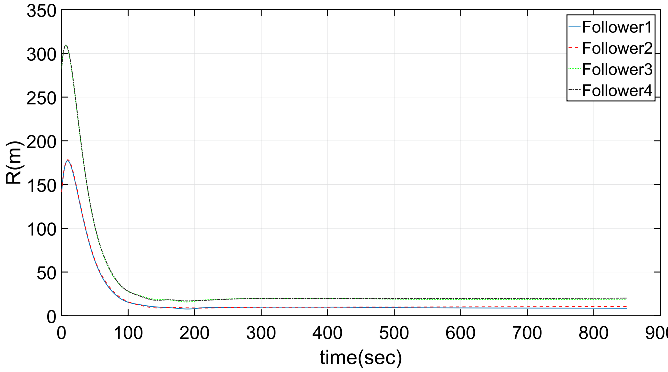

Fig. 21. Relative distance history between individual followers and leader for multiple commands.

4.4. *Results with sequential multiple path commands*

In this section, multiple path commands are issued to the leader. Here, the leader performs sinusoidal motion followed by longitudinal climbing motion followed by a circular loop in triangular formation is a shown in Fig. 5. The 3D and 2D plots when the leader is given multiple commands in a triangular formation are given in Figs. 19 and 20. The objective for doing the triangular formation is to demonstrate that the transients brought to the system due to command changes to the leader during its flight do not affect the performance of the overall system. It can be seen from Figs. 21, 22 and 23 that at the point where command changes short period transients appear and die out. From Figs. 24 and 25, one can see that the control values are well within the bounds even if the command given was so divergent.

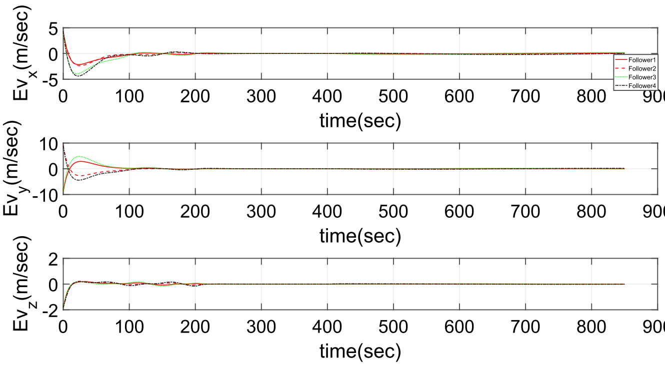

Fig. 22. Error in velocity components between leader and two followers for multiple commands.

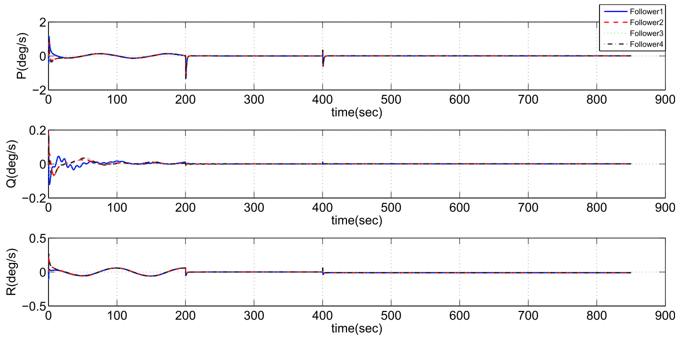

Fig. 23. Angular rates for multiple commands.

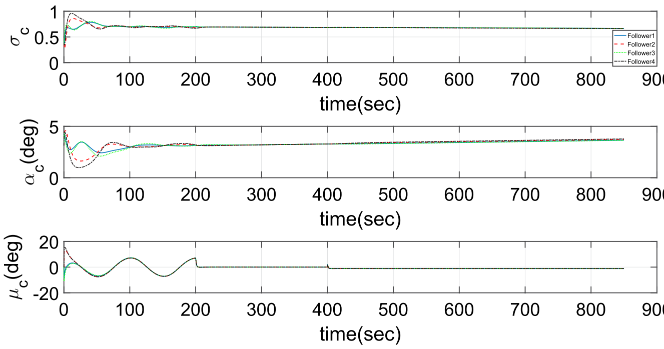

Fig. 24. Thrust, Angle of attack and Bank angle of UAVs for sequential multiple commands.

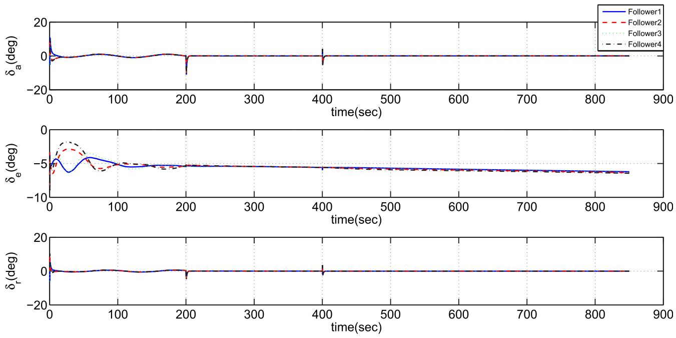

Fig. 25. Elevator, aileron and rudder deflections for multiple commands.

5. Conclusion

An innovative autonomous formation flight algorithm is proposed in this paper utilizing the nonlinear differential geometry based control theory (which is also known as "dynamic inversion"). The formation commands which are generated by the leader in its velocity frame involves the use of nonsingular rotations and transformations in terms of nonsingular quaternion parameters. The followers are then guided to those desired points, while simultaneously making sure about the alignment of their velocity vectors in appropriate directions that is favorable to maintain the formation. Moreover, the obtained guidance commands are realized for a more practical six-DOF model of the same UAV by generating desired body rate commands and then finally by generating control surface deflections. A significant advantage of this proposed problem formulation is the fact that it is "singularity-free" and does not impose any condition on the nature of the motion of the leader. This pioneering formulation makes it easier to maintain the formation once it is achieved, regardless of leader's dynamic and care-free behavior of the leader. This is because the desired rate of change of the velocity vector of the followers due to rotation of the velocity vector of the leader has been properly accounted for in the problem formulation.

Acknowledgment

This work has been carried out at ICGEL, Department of Aerospace Engineering, Indian Institute of Science, Bangalore, India. The authors would like to acknowledge Shyam Mohan M., a former Project Associate in the lab, for useful technical discussions in connection with the problem.

References

[1] F. R. Hainsworth, Induced drag savings from ground effect and formation flight in brown pelicans, *J. Exp. Biol.* **135**(1) (1998) 431–444.

[2] W. Blake and D. Multhopp, Design, performance and modeling considerations for close formation flight, in *Proc. 1999 AIAA Guidance, Navigation and Control Conference*, Portland, OR (1999), pp. 476–486.

[3] M. Pachter, J. J. D'Azzo and J. L. Dargan, Automatic formation flight control, *J. Guid. Control Dyn. AIAA* **17**(6) (1994) 1380–1383.

[4] J. D. Wolfe, D. F. Chichka and J. L. Speyer, Decentralized controllers for unmanned aerial vehicle formation flight, in *Proceedings of AIAA Guidance, Navigation, and Control Conf.*, San Diego, CA (1996).

[5] D. F. Chichka, J. L. Speyer and C. G. Park, Peak-seeking control with application to formation flight, in *Proc. IEEE Conf. Decision and Control*, San Diego, CA (1999).

[6] T. J. Koo and S. M. Shahruz, Formation of a group of unmanned aerial vehicles, in *Proc. American Control Conf.*, Arlington, VA (2001), pp. 69–74.

[7] R. V. R. Padhi and P. R. Rakesh, Formation flying with nonlinear partial integrated guidance and control, *IEEE Trans. Aerospace Electronic Systems* **50** (2014) 2847–2859.

[8] D. Enns, D. Bugajski, R. Hendrick and G. Stein, Dynamic inversion: An evolving methodology for flight control design, *Int. J. Control* **59**(1) (1994) 71–91.

[9] V. Surendra nath, S. P. Govindaraju, M. S. Bhat and C. S. N. Rao, Configuration development of all electric mini airplane, Technical Report, Project Report (Ref. No: ADEO/MAE/VSU/001), Department of Aerospace Engineering, Indian Institute of Science, Bangalore, India (2004).

[10] C. Chawla and Padhi, Neuro-adaptive augmented dynamic inversion based PIGC design for reactive obstacle avoidance of UAVs, in *Proc. AIAA Guidance, Navigation, and Control Conf.*, Portland, OR (2011).

[11] P. R. Rakesh and R. Padhi, Formation flying of uavs with dynamic inversion based partial integrated guidance and control, in *Proc. AIAA Guidance, Navigation and Control Conf.*, Portland, OR (2011).

[12] S. P. Singh, Autonomous landing of unmanned aerial vehicles, Msc Thesis, Department of Aerospace Engineering, Indian Institute of Science, Bangalore, February 2009.

[13] S. P. Singh and R. Padhi, Automatic path planning and control design for autonomous landing of UAVs using dynamic inversion, in *Proc. American Control Conference*, St. Louis, USA (2009), pp. 2409–2414.

[14] D. G. Hull, *Fundamentals of Airplane Flight Mechanics* (Springer, 2007).

[15] B. Stevens and F. Lewis, *Aircraft Control and Simulation*, 2nd edn. (J. Wiley & Sons, 2003).

[16] F. L. Markley, Unit quaternion from rotation matrix, *J. Guid. Control Dyn.* **31**(2) (2008) 440–442.

[17] J. L. Junkins and J. D. Turner, *Optimal Spacecraft Rotational Maneuvers* (Elsevier, 2012).

Arti Kalra is currently an undergraduate student in the Department of Aerospace Engineering, PEC University of Technology, Chandigarh, India. This work was carried out during her stay as a research intern at Indian Institute of Science, Bangalore.

She is a member of Aeronautical Society of India and Aero Modelling Society, PEC University of Technology, Chandigarh. She has also worked in MAV Laboratory in Indian Institute of Technology, Kanpur as a research intern. Her research interests include guidance and control of Unmanned Aerial Vehicles. She is also keen to work with the guidance and control algorithms for space vehicles.

Sreenatha Anavatti is a senior lecturer with SEIT, UNSW Canberra, Australia. Before moving to Australia in 1998, he was with Indian Institute of Technology Bombay, Mumbai, as an Associate Professor.

His research interests involve the application of artificial intelligence techniques like Fuzzy and Neural systems for UAVs, Underwater Vehicles and Ground Vehicles. The research interests include Identification of dynamic systems, Control of dynamic systems, Navigation and Path planning for autonomous vehicles, Evolutionary Fuzzy systems and their applications to dynamic systems. He has supervised a number of Ph.D. scholars over the years.

Radhakant Padhi is currently working as a Professor in the Department of Aerospace engineering, Indian Institute of Science, Bangalore. He did Ph.D. in Aerospace Engineering from Missouri University of Science and Technology – Rolla, USA in 2001 and continued there as a postdoctoral fellow for two more years. In 2003, he joined the Indian Institute of Science and is continuing over there since then. Dr. Padhi is an Associate Fellow of American Institute of Aeronautics and Astronautics (AIAA), a Senior Member of IEEE and a Council member of the International Federation of Automatic Control (IFAC). He is a member of Technical Committees on Aerospace in both IEEE and IFAC as well as a member of the IFAC Technical Committee on Mechatronics.

Dr. Padhi's main research interest is on synthesis algorithms in optimal and nonlinear control as well as state estimation. He works on diverse application areas such as control and guidance of aerospace vehicles, mechanical systems, distributed parameter systems, biomedical systems and industrial process control. He has over 210 publications in international journals and conferences and has received many awards and honours for his research contributions. As a member of the technical review committee for Defense R&D Organisation (DRDO) and Indian Space Research Organisation (ISRO), he has reviewed several projects of national importance in India.